THE JOURNAL OF PHYSICAL CHEMISTRY A

Article

Cite This: J. Phys. Chem. A 2018, 122, 2468−2478

pubs.acs.org/JPCA

Hydrophobic Collapse in *N*-Methylacetamide−Water Mixtures

Published as part of The Journal of Physical Chemistry virtual special issue "Time-Resolved Vibrational Spectroscopy".

Evgeniia Salamatova,[†] Ana V. Cunha,[†] Robbert Bloem,[‡,§] Steven J. Roeters,[‡] Sander Woutersen,[‡] Thomas L. C. Jansen,[†] and Maxim S. Pshenichnikov*[,†]

[†]Zernike Institute for Advanced Materials, University of Groningen, Nijenborgh 4, 9747 AG Groningen, The Netherlands

[‡]Van 't Hoff Institute for Molecular Sciences, University of Amsterdam, Science Park 904, 1098 XH Amsterdam, The Netherlands

Supporting Information

ABSTRACT: Aqueous *N*-methylacetamide solutions were investigated by polarization-resolved pump−probe and 2D infrared spectroscopy (2D IR), using the amide I mode as a reporter. The 2D IR results are compared with molecular dynamics simulations and spectral calculations to gain insight into the molecular structures in the mixture. *N*-Methylacetamide and water molecules tend to form clusters with "frozen" amide I dynamics. This is driven by a hydrophobic collapse as the methyl groups of the *N*-methylacetamide molecules cluster in the presence of water. Since the studied system can be considered as a simplified model for the backbone of proteins, the present study forms a convenient basis for understanding the structural and vibrational dynamics in proteins. It is particularly interesting to find out that a hydrophobic collapse as the one driving protein folding is observed in such a simple system.

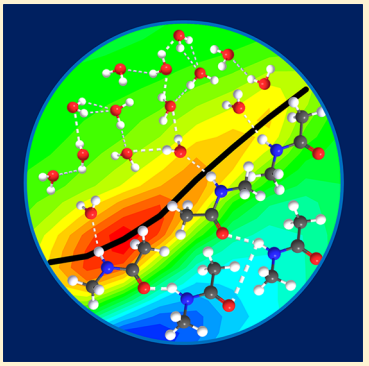

1. INTRODUCTION

The development of two-dimensional infrared (2D IR) spectroscopy[1−3] led to extensive studies of biological and biochemical systems, with structural and dynamical properties of peptides and proteins[3,4] being at the focus. Amide I (C═O stretch) vibrations were of particular interest due to their abundance in proteins and the resulting potential to access the information on structure and dynamics through their strong mutual coupling.[5−12]

The mechanism of protein folding[13] is an important subject as misfolding of proteins leads to diseases like Alzheimer's and Parkinson's disease, type II diabetes, and cancer.[14,15] Great progress in the understanding of this complex process has been made in recent years.[11,12,16−37] The folding process can be steered by proteins called chaperones,[38,39] influenced by salt bridge formation,[40] and affected by pH and ionic strength. However, overall the hydrophobic collapse[27,41] and the framework model[16] have been proposed as the most common driving forces for protein folding. Understanding these mechanisms on a fundamental level for proteins is, however, challenging as sequence-specific effects inevitably play a role as well. The idea of this paper is to study the behavior of the amide groups forming the backbone of protein chains, when mixed with water. We want to eliminate the effect of side chains to address the question to what extent the interactions between water and amide groups drive structural formation.

N-Methylacetamide (NMA) is a convenient model molecule for studying such interactions. NMA is composed of a single peptide bond[42−48] (−CONH−), which contains a single amide I mode. Due to this structure, NMA is used as a model compound for the linkage between peptide units.[44,49] NMA can both donate and accept hydrogen bonds (HBs)[50] which makes it miscible with a wide range of solvents.[42−44,48,51,52] This has led to extensive experimental[42−45,48,52] and theoretical[47,48,53−55] studies of vibrational dynamics of the amide I mode of NMA[56] in different solvents.

The studies of NMA diluted in polar and nonpolar solvents[42−45,48,51,52,54,56−65] provided important information on the relaxation pathways of the amide I mode and its spectral dynamics. An extensive study of the influence of the solvent on the amide I mode vibrational dynamics was performed by DeCamp et al.[48] The amide I lifetime appeared to be weakly dependent on the particular solvent and were reported to be 450 fs in heavy water,[44] 380 and 430 fs in heavy water and DMSO, respectively[52] (with an ∼2 ps tail reported in the latter study). In contrast, solvents that form weak HBs lead to slower HB and reorientational dynamics.[48,52] Spectral dynamics of NMA molecules diluted in water exhibit bimodal dynamics: a time scale of 50 fs was assigned to water librations, while HB vibration dephasing occurred on a 180 fs time scale.[48] Recently, NMA bulk dynamics were studied by optical Kerr effect spectroscopy[66] and theoretically and experimentally by 2D IR spectroscopy.[67] In the former study, structural relaxation was observed to occur at the time scales of 30 and 180 ps at 300

Received: January 9, 2018
Revised: February 2, 2018
Published: February 9, 2018

DOI: 10.1021/acs.jpca.8b00276
J. Phys. Chem. A 2018, 122, 2468−2478

K; both times accelerated by a factor of ∼30 at 470 K. In the latter paper, an interesting interplay between HB and vibrational coupling was reported and interpreted from the viewpoint of the existence of highly ordered HB chains where the transition dipoles are largely oriented parallel to each other along the chain of NMA molecules.

So far, the NMA dynamics have been studied for both diluted[48,52] and bulk[66,67] environments. However, in biological systems neither situation is relevant, as proteins and peptides form HBs with the aqueous surroundings. This situation can be only be mimicked by concentrated NMA−water mixtures. We will study such solutions to understand how the interactions between water and amide groups affect the HB structure and dynamics of the amide groups.

In this paper, we examine the dynamics of mixtures of NMA molecules and water with 2D IR spectroscopy and molecular dynamic simulations combined with spectral simulations. In the 50/50 molar % mixture the amide I lifetime is 450 ± 100 fs which is in line with previous studies.[43,44,67] We show that such a mixture leads to clustering of NMA and water molecules, which leads to "frozen" dynamics at the picosecond time scale. The methyl groups in the NMA clusters tend to stick together, suggesting a hydrophobic collapse. However, as evident from the anisotropy measurements, this does not fully prevent the movement of the vibrational excitations between amide I modes typical for bulk NMA, but its extent is limited to the NMA cluster size.

2. MATERIALS AND METHODS

2.1. Sample Preparation. We used NMA with deuterated peptide bonds and deuterated water (D_2O) to avoid unwanted overlap of the C═O stretching mode at ∼1650 cm^{-1} with the HOH bending mode[68] (∼1645 cm^{-1}). *N*-Methylacetamide-d_1 (NMA-d_1) with isotopic enrichment of >99% was obtained from CDN Isotopes; deuterium oxide (D_2O) with isotropic purity of >99.9% of the D atom was purchased from Sigma-Aldrich. Both chemicals were used without any further purification.

NMA-d_1 is a solid at the room temperature (∼22 °C), so it was placed on a heating plate of 40 °C until it was completely melted. After that, liquid NMA-d_1 was mixed with D_2O in precalculated volumes in order to obtain mixtures with variable mole fractions of NMA-d_1 (hereinafter the mole fraction of NMA in solution is denoted as X;[69] i.e., X = 1 and X = 0 correspond to pure NMA-d_1 and heavy water, respectively). Approximately 1.5 μL of the NMA-d_1/D_2O solution was squeezed between two 1 mm thick CaF_2 windows, which were preheated up to T = 40 °C to ensure homogeneous distribution of the sample all over the area. In order to minimize the contact of the samples with air, the assembly was placed in a sealed cylindrical sample holder. The sample thickness (estimated from the absorbance) was ∼3 μm assuming that the solution was spread uniformly between the 1 inch diameter CaF_2 windows.

To avoid any contact with air moisture, sample preparation was performed under nitrogen atmosphere. During the experiments, to avoid potential crystallization of NMA-d_1 at high concentration, the temperature of samples were uniformly maintained at temperature of 30.5 ± 1 °C by a thermostat controlled by a thermocouple.

2.2. IR Spectroscopy. An FTIR-spectrometer Vertex-70 purged with dry nitrogen was used for recording the FTIR absorption spectra in the spectral range of 1550−1750 cm^{-1}. The spectral resolution was ∼2 cm^{-1}; 32 scans were averaged for every absorption spectrum. The maximal OD in the region of interest was ∼0.6.

An interferometer platform used as a base for the collinear 2D IR setup is described elsewhere.[70] In short, an IR pulse (∼25 μJ of energy, 135 fs in duration, 140 cm^{-1} fwhm spectral width) centered at 1640 cm^{-1} was split into two pumps (90% of the total intensity) of equal intensity, probe and reference. The time difference between probe and reference pulses was set at 40 ps to avoid any interference. A wobbler in the probe beam path generated a $-\pi$, 0, $+\pi$, 0 phase sequence[71] for subsequent pulses (1 kHz repetition rate) to remove sample scattering. Before the sample the polarization of the pump was rotated by a $\lambda/2$ waveplate by 45° with respect to the pump polarization. After the sample, either the parallel or the perpendicular polarization component of the probe beam was selected by a polarizer. The probe spectrum was detected by one of the 2 × 32 pixel MCT array rows (Infrared Associates) to provide the ω_3 dimension of the 2D spectra. Detection of the reference beam spectrum was carried out by the second array row of the MCT spectrometer. To increase the signal-to-noise ratio, the probe spectrum was normalized by the reference spectrum for each laser shot. At fixed waiting times T between the probe and the latest pump pulse the delay between two pump pulses, t_1, was scanned up to 2 ps with fast scanning approach.[70] The normalized probe spectrum was averaged over the wobbler-generated phase sequence to extract the nonlinear response related to all three pulses (two pumps and the probe), zero-padded to 4 ps, and Fourier-transformed to obtain the ω_1 dimension with the phase correction applied.[72] For the pump−probe measurements, one of the pump beams was used.

The interferometer and the sample and detection compartments of the setup were purged with dry air to prevent water peaks in the IR spectrum and to minimize the sample adsorption of the water vapor.

2.3. Theory. The molecular modeling simulations were performed with the GROMACS suite 4.6.1[73] using a combination of the OPLS-AA[74] force field and the SPC/E water model[75] to describe the NMA/water mixture, with variable NMA/water content. The production run of 1 ns at 27 °C was performed at constant volume and the coordinates of all atoms using 1 fs time steps. Snapshots were stored at each 10 fs for analysis and spectral modeling. The temperature was kept constant using the Berendsen thermostat,[76] and a 1.1 nm cutoff was used for both Lennard-Jones and Coulomb interactions. The truncation of the Lennard-Jones potential was compensated by introducing analytical corrections to pressure and potential energy.[77] The long-range Coulomb interactions were treated using particle mesh Ewald method, with a grid step of 0.16 nm and a convergence of 10^{-5}.[78] All bonds were constrained using the LINCS algorithm.[79]

The spectral modeling was performed using the numerical integration of Schrödinger equation (NISE) method.[49,80] The time dependent Schrödinger equation was solved numerically for the time-dependent amide I Hamiltonian:

$$H(t) = \sum_{i}^{N} \omega_i(t) B_i^{\dagger} B_i - \frac{\Delta}{2} \sum_{i}^{N} B_i^{\dagger} B_i^{\dagger} B_i B_i + \sum_{i \neq j}^{N} J_{ij}(t) B_i^{\dagger} B_j - \sum_{i}^{N} \vec{\mu}_i(t) \cdot \vec{E}(t) (B_i^{\dagger} + B_i) \quad (1)$$

DOI: 10.1021/acs.jpca.8b00276
J. Phys. Chem. A 2018, 122, 2468−2478

where $B_i^\dagger$ and B_i are the bosonic creation and annihilation operators, $\omega_i(t)$ is the time dependent fundamental amide I frequency for the ith molecule, and $\vec{\mu}_i(t)$ is the corresponding transition dipole. The anharmonicity, Δ_i, was kept constant at 16 cm^{-1}.[44] The amide I site frequencies, $\omega_i(t)$, were calculated using the Jansen electrostatic map,[53] which was reported to work well with the OPLS-AA force field.[81] The long-range couplings between the different amide I units were calculated using the transition charge coupling (TCC) model,[8,55] where a charge, q_n, and a transition charge, dq_n, and a normal mode coordinate, $\vec{\nu}_{n_i}$, are assigned to each atom of the amide I unit. The TCC model has the form

$$J_{ij} = \frac{1}{4\pi\varepsilon_0}\sum_{n,m}\left(\frac{dq_n dq_m}{|\vec{r}_{n_i m_j}|} - \frac{3q_n q_m(\vec{\nu}_{n_i}\cdot\vec{r}_{n_i m_j})(\vec{\nu}_{m_j}\cdot\vec{r}_{n_i m_j})}{|\vec{r}_{n_i m_j}|^5} - \frac{dq_n q_m \vec{\nu}_{m_j}\cdot\vec{r}_{n_i m_j} + q_n dq_m \vec{\nu}_{n_i}\cdot\vec{r}_{n_i m_j} - q_n q_m \vec{\nu}_{n_i}\cdot\vec{\nu}_{m_j}}{|\vec{r}_{n_i m_j}|^3}\right) \quad (2)$$

Here, the subscripts n and m are the number the atoms that belong to different amide I local modes at molecules i, and j, respectively. The distance vector between two atoms in the involved molecules is given by $\vec{r}_{n_i m_j}$. The values of the parameters used are given in ref 18.

3. RESULTS AND DISCUSSION

3.1. Linear Absorption. The experimental and theoretical linear absorption spectra of the NMA-d_1/D_2O mixtures studied are shown in Figure 1. The experimental and theoretical spectra

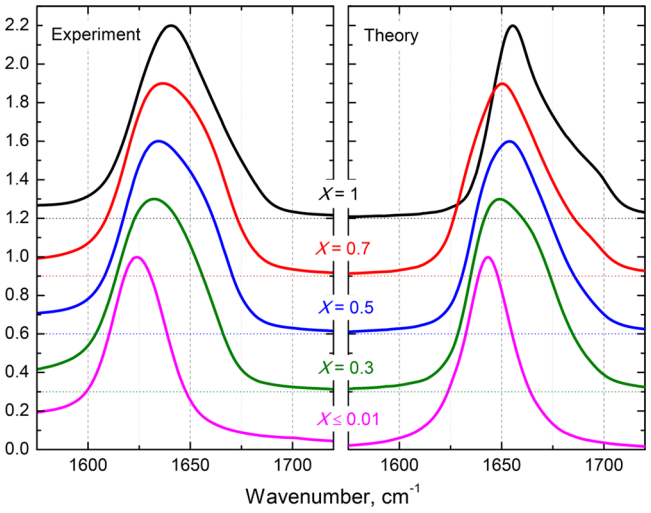

Figure 1. Comparison of linear experimental (left panel) NMA-d_1/D_2O mixtures and simulated (right panel) NMA/water absorption spectra at different molar fractions. The mole fraction X of NMA-d_1 is shown next to the corresponding spectrum.

demonstrate similar trends: with increasing NMA-d_1 concentration, the spectra are blue-shifted, become broader at intermediate concentrations, and narrow down in diluted NMA solutions. Both pure NMA spectra exhibit a high-frequency shoulder, which was earlier shown to have mixed HB–vibrational coupling origin.

The experimental spectra at X = 0.5–0.7 also show a noticeable high-frequency sub-band, while its appearance in the theoretical spectra is not as noticeable except for the X = 0.3 case. The discrepancy most probably originates from the fact that the applied force fields overestimate the NMA clustering, which leads to more heterogeneity of the solution. Therefore, in what follows we have chosen to compare the experimental spectra of the X = 0.5 mixture with X = 0.3 of the simulated mixture (Figure 2) as representing the most similar heterogeneous case.

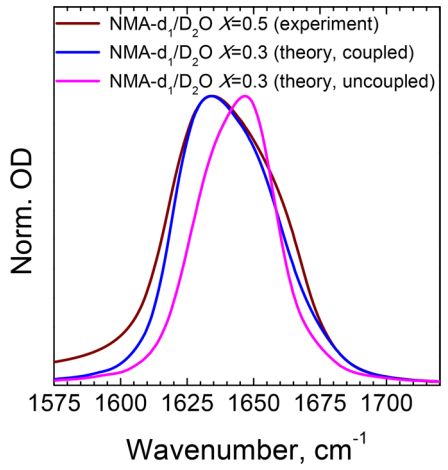

Figure 2. Linear FTIR spectrum of the NMA-d_1/D_2O solution (wine, X = 0.5) in comparison with the simulated coupled (blue) and uncoupled (magenta) spectra at X = 0.3.

To disentangle the origin of the main NMA band and the high-frequency sub-band, the linear spectrum of the exact same system was calculated with the vibrational coupling between amide I modes set to zero (Figure 2). The spectra with zero coupling (hereafter denoted as uncoupled) are narrower and blue-shifted by ~13 cm^{-1} in comparison with the coupled spectra. This indicates a strong effect of vibrational coupling on the spectral line shape as was previously reported for bulk NMA.[67] The high-frequency sub-band vanishes, which suggests that the sub-band originates from the vibrational coupling.

To verify this conclusion, all possible types of HB between NMA and water were extracted from the MD simulations. Geometric criteria[82] were used to determine if HBs were present between the molecules. For water–water and water–NMA HBs a common criterion defined for water[83] was used, while the criterion described in ref 67 was used for NMA–NMA HBs. In total, there are 21 types of HB species (see the Supporting Information, section 1), which can be further categorized into three main groups according to the number of accepted HBs. Group I includes the free NMA (f-NMA) and NMA donating one HB (1d-NMA). The species in group II either accept one HB (1a-NMA) or donate one and accept one HB (1a-1d-NMA). Group III is characterized by two accepted HBs (2a-NMA) or two accepted and one donated HBs (2a-1d-NMA). No difference with respect to the origin of the HB donor (water or NMA) is made in this group categorization. The fraction of each group is depicted in Figure 3; group II is by far the most populated one.

To estimate the effect of the intermolecular coupling to the spectral features, the linear absorption spectra for each group were calculated in the static approximation for both coupled and uncoupled cases (Figure 4). The central frequency of group I is the most blue-shifted because of similarity of the effect of

DOI: 10.1021/acs.jpca.8b00276
J. Phys. Chem. A 2018, 122, 2468–2478

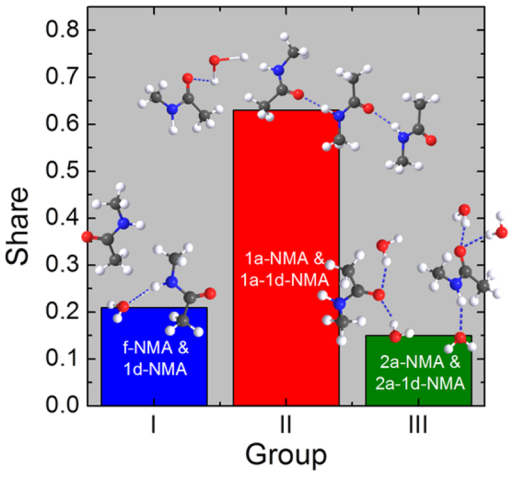

Figure 3. Fraction of each NMA-d_1/D_2O group. The number of accepted−donated HBs in the group is shown in the bar. Above the bar, representative corresponding structures are depicted.

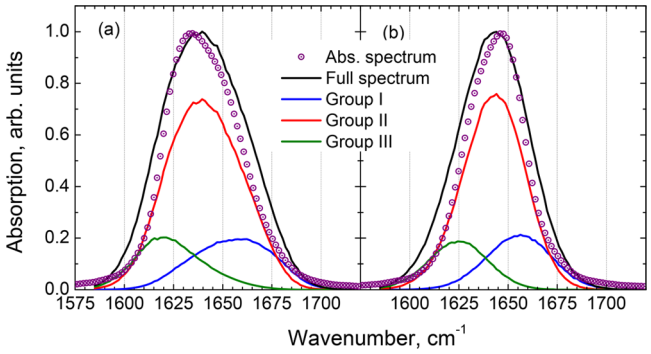

Figure 4. Linear absorption spectra in a static approximation of each group for coupled (a) and uncoupled (b) cases. For comparison, the full dynamic spectra from Figure 2 are also shown by the circles.

HB donation and no HB on the frequency of the C═O oscillator. In contrast, for group III the central frequency is the most red-shifted due to two accepted HBs. The dominant single HB accepting species (group II) absorbs at a frequency in the middle of the band. Of course, this is true only for the central frequencies: due to the broadness of the spectral distributions, there are double HB accepting complexes (group III) of which the frequency is blue-shifted as compared to free NMAs in group I and vice versa.

For each group the vibrational coupling leads to broadening of the spectra due to additional inhomogeneity in the coupling strengths (compare Figure 4a and Figure 4b), similar to the observation in bulk NMA.[67] However, the red shift of the coupled spectra does not exceed 4−5 cm^{-1}, which is substantially lower than the 13 cm^{-1} red shift seen in the full dynamical calculations (Figure 2). This is because when calculating the static spectra for the different groups, the coupling between species belonging to different groups is neglected. Therefore, the similarity of the static structures tells us that the coupling between molecules belonging to different groups determines the shift in the dynamics spectra, and therefore the molecules belonging to the same group are dispersed throughout the liquid. A comparison between full static spectra and linear absorption spectra simulated with the NISE approach (i.e., accounting for motional narrowing effects) shows that the HB dynamics lead to narrowing of both the coupled and uncoupled spectra, hereby proving the importance of the motional narrowing effects.

In principle, the uncoupled spectra in Figure 2 could be obtained experimentally by using isotopically diluted NMA where the carbonyl carbon or oxygen is replaced by ^{13}C and/or ^{18}O which leads to red-shifting of the amide I absorption by 20−60 cm^{-1}.[84] This is comparable to typical values of vibrational couplings of <20 cm^{-1},[85] so the intermolecular coupling is not fully suppressed.

3.2. Pump−Probe. To extract the amide I mode lifetime, the frequency-dependent isotropic component of the pump−probe signal was extracted from the experimental spectra as

$$I_{iso}(t) = \frac{I_{\parallel}(t) + 2I_{\perp}(t)}{3} \quad (3)$$

where $I_{\parallel}(t)$ and $I_{\perp}(t)$ are the parallel and perpendicularly polarized components, respectively, of pump−probe signal with respect to the pump. The isotropic transient spectra for an NMA-d_1/D_2O mixture with $X = 0.5$ recorded at several pump−probe delays are shown in Figure 5. The transient spectra

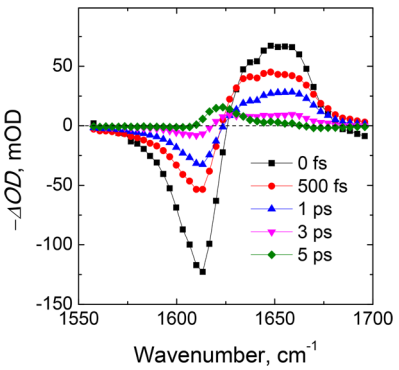

Figure 5. Isotropic transient spectra of $X = 0.5$ NMA-d_1/D_2O mixture at different delay times (as shown in the legend).

consist of a positive bleaching component (at ∼1650 cm^{-1}) and a negative induced absorption component (at ∼1615 cm^{-1}). The transient spectrum at 5 ps is drastically different from those at shorter times. This is ascribed to thermal effects[86] that begin to dominate the pump−probe signal at longer times.

To determine the time scales of the population relaxation and thermalization, we used the isotropic pump−probe transients at the extreme points of bleaching/stimulated emission (∼1650 cm^{-1}) and induced absorption (∼1615 cm^{-1}) frequencies, along with the transient near the compensation point at ∼1625 cm^{-1} (Figure 6). The latter represents the thermalization signal that is the least affected by the population dynamics. Its setup time of 4.2 ± 0.3 ps is apparently much longer than the population relaxation time, which hints that a four-level model[87] (with the ground, excited, intermediate, and hot-ground states) should be used to describe the transients. The lifetime of amide I mode calculated from such a model amounted to ∼450 ± 100 fs. While the obtained lifetime of the amide I mode corroborates the previous results, it might be affected by the presence of HB configurations with different lifetimes and mixing up frequencies of excited-state absorption and bleaching/stimulated emission of these species. Nonetheless, the value of 450 fs is sufficiently reliable for estimating the time window provided for 2D IR experiments (∼1.5 ps).

DOI: 10.1021/acs.jpca.8b00276
J. Phys. Chem. A 2018, 122, 2468−2478

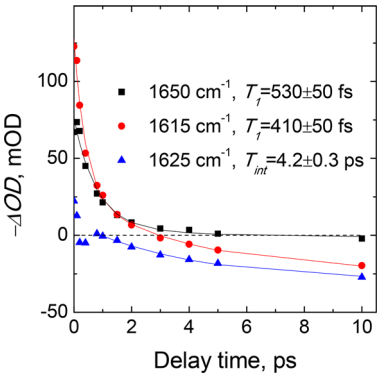

Figure 6. Representative pump−probe transients of X = 0.5 NMA-d_1/D_2O mixture at the maximum of bleaching/stimulated emission (black symbols), induced absorption (red symbols), and the compensation point (blue symbols). The fits obtained from the four-level thermalization model are shown by the solid lines; the respective relaxation times (the excited state lifetime T_1 and the thermalization time T_{int}) are given in the legend. The sign of the 1615 cm^{-1} transient was inverted to allow easy comparison with the other transients.

3.3. 2D IR Spectroscopy. The linear spectrum does not contain any information about the NMA-d_1/D_2O dynamics. Such information can be extracted from nonlinear 2D spectra (Figure 7). All spectra are strongly elongated along the diagonal, which suggests "frozen" dynamics. However, more careful inspection reveals the presence of two peaks with central frequencies at ∼1635 cm^{-1} and ∼1660 cm^{-1} (see the linear spectra in Figure 2 for comparison). Therefore, the diagonal elongation might result from a simple combination of the two peaks each of which is not necessarily elongated diagonally (providing there is no chemical exchange between the peaks; see the Supporting Information, section 2). Hence, we decided to perform the center line slope (CLS)[88,89] analysis in two separate regions which correspond to the two peaks in Figure 2.

In the low-frequency region (Figure 8a), the experimental CLS values at short times are about 0.55 which indicates a substantial contribution of the homogeneous broadening, in accordance with the theoretical calculations. Most probably, this broadening originates from fast bath modes, such as the water librations. In contrast, the CLS values at short times in the high-frequency region (Figure 8a) are close to unity, indicating that this region of the spectrum is primarily inhomogeneously broadened (see Figure 4 and the discussion around it). The small rise at short waiting times most probably originates from the pulse overlap region and/or nonresonant (instantaneous) background response.

The theoretical CLS values in the low-frequency region capture the experimental ones rather well (Figure 8a). However, the theory predicts more homogeneity in the high-frequency region (Figure 8b); this may in part be due to the overestimation of vibrational couplings[81,90] (which is supported by the fact that the CLS values are higher when the coupling is set to zero; see Figure 8) and overestimation of frequency fluctuations of the free species. The latter likely arises as the molecular polarizability in the point charge based force fields used here are accounted for by scaled point charges to match the average dipole moment in the liquid and configurations far from this average are described less accurately.[54,75] We also note that the coexistence of free and clustered NMA molecules might lead to a vibrational lifetime in the low-frequency region that differs from the lifetime in the high-frequency region (see discussion in section 3.2).

At the main peak position the CLS values for the uncoupled simulations are generally higher than for the simulations accounting for the coupling (Figure 8a). In the high-frequency

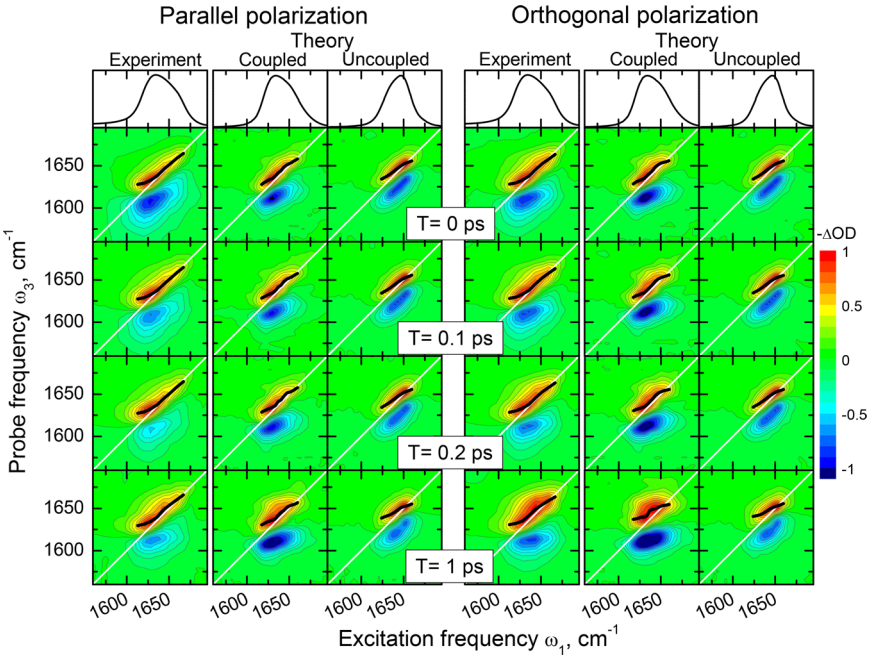

Figure 7. Normalized 2D IR spectra of X = 0.5 NMA-d_1/D_2O mixture at several representative waiting times T. The experimental (the left-hand columns) and the simulated coupled and uncoupled (the middle and right-hand columns, respectively) spectra are shown for parallel and orthogonal polarization arrangement. Red and blue colors represent the bleaching/stimulated emission and induced absorption, respectively. The equidistant contours are drawn with 10% steps from the maximal amplitude. The thick black lines show the results of the CLS analysis in the following frequency regions: experiment 1613 < ω_1 < 1667 cm^{-1}, theory (coupled) 1617 < ω_1 < 1660 cm^{-1}, and theory (uncoupled) 1624 < ω_1 < 1660 cm^{-1}.

DOI: 10.1021/acs.jpca.8b00276
J. Phys. Chem. A 2018, 122, 2468−2478

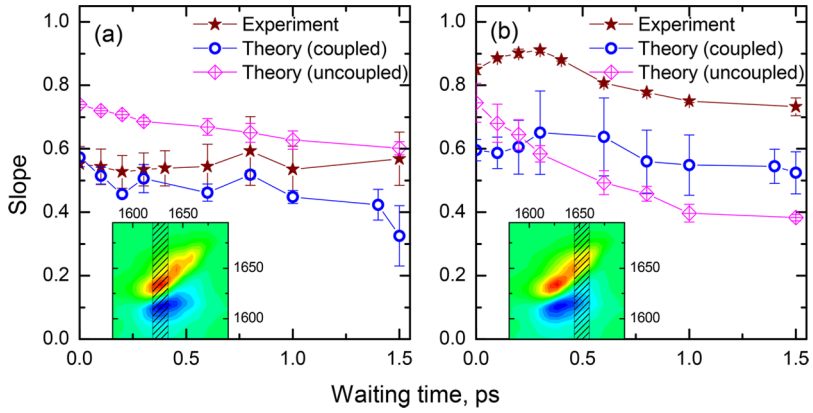

Figure 8. CLS analysis of the 2D spectra (parallel polarization) in the amide I mode region performed at the low (experiment, coupled, 1620 < ω_1 < 1636 cm^{-1}; uncoupled, 1633 < ω_1 < 1648 cm^{-1}) and high (experiment, coupled, 1644 < ω_1 < 1659 cm^{-1}; uncoupled, 1656 < ω_1 < 1670 cm^{-1}) frequencies. The region of the CLS analysis is shown in the inset as a shaded area. Theoretical values are computed for the coupled case (blue circles) and uncoupled (magenta diamonds).

region the CLS values are much more similar (Figure 8b). This suggests that the couplings are more important for the NMA molecules involved in HB. One must of course keep in mind that when the coupling is included, the excitations are no longer localized on a specific HB type.

For all waiting times, the experimental and theoretical CLS values do not change substantially in both frequency regions, which suggests "frozen" dynamics of the amide I mode at the picosecond time scale. Such "frozen" dynamics have been reported earlier for water in reversed micelles[91] and around hydrophobic groups.[92] This effect was explained as breakage of the 3D HB network among the water molecules. As we concluded from the analysis of the static spectra (Figure 4), different types of HB species are dispersed in the mixture. From 2D spectroscopy, we inferred that the dispersed structures are static at least at the time scale of a few picoseconds. This situation is visualized in Figure 9 where a snapshot from MD simulations clearly shows the phase separation of the mixture onto NMA clusters (in the center) surrounded by the water molecules (at the periphery).

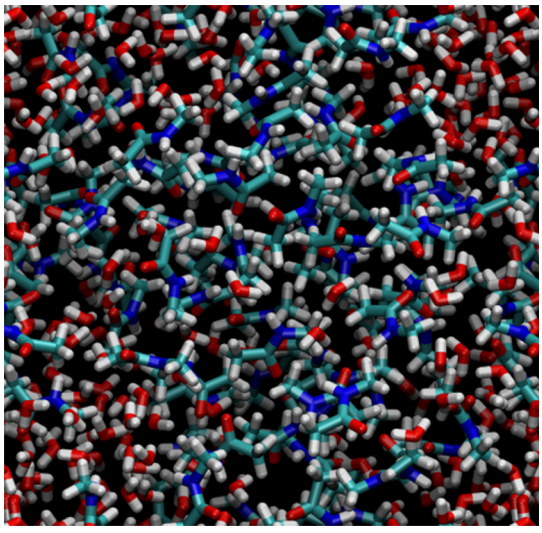

Figure 9. Snapshot from the MD simulation of the NMA–water mixture. Oxygen atoms are shown in red, hydrogen atoms in white, carbon atoms in cyan, and nitrogen atoms in blue.

To quantify the clustering effect, we calculated the joint angular–radial distribution functions (JARDFs) of the NMA/water mixture and compared them with JARDFs of bulk NMA (Figure 10). The initial peak at ∼0.48 nm corresponds to HBs between amide units in the first solvation shell. After this, the JARDF for NMA contains apparent recurrences, in both the radial and angular dependences, which are also presented in less pronounced form in JARDF of the mixture.

The features of the JARDF revealing the liquid structure are highlighted in Figure 11 where two particular cuts of the JARDFs are depicted, one in the radial direction at a fixed angle and another one at an angle direction at a fixed distance. The main peak of the bulk NMA JARDF has a higher amplitude than its mixture counterpart, which reflects more ordering among HBs between amide units already in the first solvation shell. Furthermore, several recurrences follow that correspond to HBs between amide units in the second and third solvation shells. This is not surprising given the previous findings that NMA in bulk forms chain-like structures with well-defined orientation of the HBs between amide units.[67] These features are less pronounced in the NMA–water mixture, lending additional support for the system heterogeneity. The radial cut shows a similar trend: a relatively narrow (∼50°) distribution of C═O angles for bulk NMA and a much broader (∼65°) distribution for the NMA–water mixture. These observations lead to the conclusion that the NMA–water mixture is not as well-organized as bulk NMA and that the formation of the HB chains of NMA molecules is largely destroyed by water molecules.

The nanoscopic phase separation in the mixture can also be interpreted from the perspective of water molecules (Figure 12). The radial distribution function (RDF) for O···O distances of the NMA–water mixture has a higher amplitude initial peak and stronger recurrences than the RDF of bulk water.[93] This indicates that the water molecules in the mixture form extended clusters, with a better defined water structure than in the bulk. This is well in line with many reported studies of water at molecular interfaces.[94−98]

To further quantify the clustering of NMA molecules, the RDF between methyl groups (C···C distance) of the NMA molecules were calculated (Figure 13) and compared with that of bulk NMA. The probability of finding two NMA methyl groups at a distance of 0.38 nm distance is higher in the mixture compared to bulk NMA. This makes us conclude that in the

DOI: 10.1021/acs.jpca.8b00276
J. Phys. Chem. A 2018, 122, 2468−2478

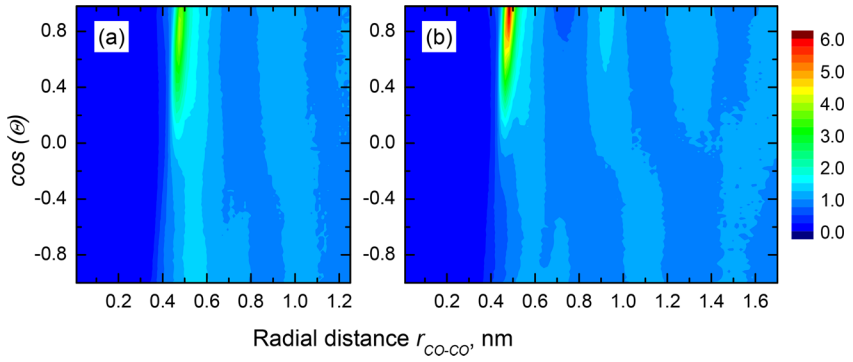

Figure 10. Joint angular−radial distribution functions of (a) NMA−water mixture and (b) bulk NMA. Θ is the angle between the pairs of C═O bond vectors (cos(Θ) = 1 and cos(Θ) = −1 for the parallel and antiparallel bond vectors, respectively), and $r = r_{CO-CO}$ is the distance between the centers of pairs of C═O bonds. The color map corresponds to the occurrence of formation of the pair of C═O bonds: the red color shows the high occurrence, while the blue is used for low occurrence. Both distributions are normalized to unity at large r.

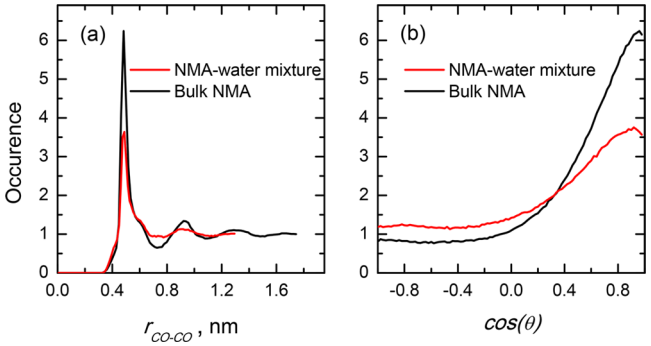

Figure 11. (a) Radial distribution function of NMA mixture and bulk NMA at cos(Θ) = 1 and (b) angular distribution function of dissolved and bulk NMA at r = 0.48 nm.

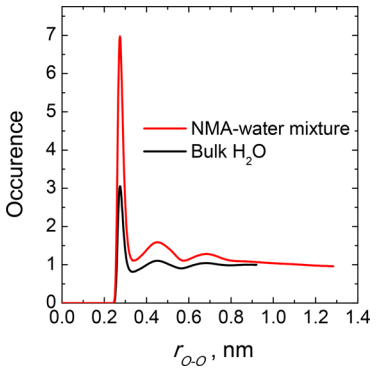

Figure 12. Radial distribution functions of water oxygen for NMA−water mixture (red) and bulk water (black). Both distributions are normalized to unity at large r.

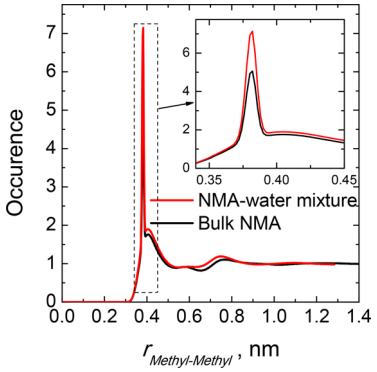

Figure 13. Methyl−methyl RDF of NMA−water mixture (red) in comparison with bulk NMA (black). Both distributions are normalized to unity at long distances r.

mixture, the NMA molecules tend to form clusters in which the hydrophobic methyl groups stick together. This, thus, resembles the hydrophobic collapse observed in the protein folding process,[27] but in this case it is solely driven by the presence of the small methyl groups in the NMA molecule instead of the large hydrophobic side chains present in real proteins.

To verify the destabilizing effect of water on the structural order of NMA, we measured and calculated the anisotropy decay (Figure 14). Both the experimental and calculated coupled anisotropies decay much faster than the rotational correlation function (RCF) but with the same rate as the population transfer regardless the spectral region. This is in a sharp contrast with bulk NMA where the anisotropy decays faster than RCF but slower than the population transfer. The latter was interpreted as vibrational excitation moving through the transition dipole network ordered by HBs. Apparently, the current situation is very different: the vibrational excitation is still mobile (the anisotropy decays faster than RCF), but the orientations of the transient dipole moments are not mutually aligned so that the anisotropy is quickly scrambled. The vibrational excitation in the mixture is delocalized over 8.6 NMA molecules on average as compared to 42 in the bulk[67] (as determined using the inverse participation ratio[99]). In the mixture, the delocalization is thus strongly reduced as it has to be localized inside the NMA cluster. All these observations confirm our conclusion that water induces a hydrophopic collapse in NMA destabilizing the intermolecular HBs and lowering the structural order.

4. CONCLUSIONS

In this paper, we have studied NMA−water mixturess with linear and nonlinear IR spectroscopy. The lifetime of the amide I mode has been found to be similar to the previous reports of diluted and the bulk NMA solutions. We revealed that adding water to NMA leads to disruption of the HB chains of NMA molecules, which were recently reported to be present in bulk NMA.[67] Instead, solvation results in the formation of water and NMA clusters where the amide I dynamics are “frozen”, at least at the picosecond time scale. Curiously, only the frequency and

DOI: 10.1021/acs.jpca.8b00276
J. Phys. Chem. A 2018, 122, 2468−2478

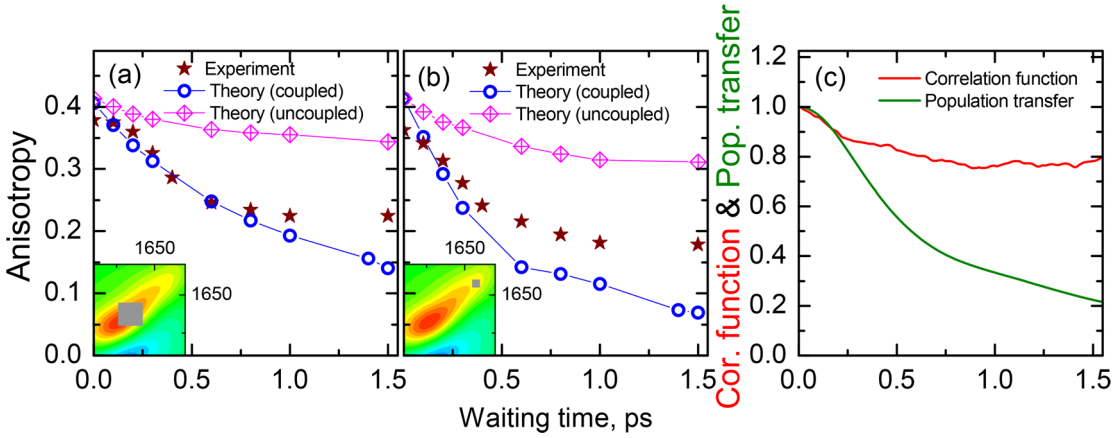

Figure 14. Anisotropy decay of the main (a) and high-frequency (b) absorption peaks for experimental and theoretical spectra. The anisotropy values were calculated from the integration of the 2D spectra over the region shown in the corresponding inset; for the uncoupled case, the spectral area around the main peak at ∼1650 cm^{-1} (Figure 2) was taken. (c) Rotational correlation function (RCF) and population transfer function obtained from MD simulations. Note that the uncoupled case produces the anisotropy decay similar to the RCF as expected from the localized (immobile) vibrational excitation.

rotational dynamics are frozen while the anisotropy is not and does decay at the ∼1 ps time scale. This is because the excitation is mobile and therefore samples a few amide I modes with similar frequencies but different orientations. The former leads to constant CLS values (after the initial drop), as the excitations tend to be shared between vibrations with similar frequency, while the latter results in the anisotropy decay. It would be interesting to investigate if the water dynamics are frozen, too (similar to the recently reported "mayonnaise effect"[100]); these experiments are underway.

In our opinion, the results obtained here could form a basis for understanding the hydration structure and (vibrational) dynamics of more complex biological systems than the NMA−water system studied in the current work. Real proteins may, for example, have charged groups at the surface, a complication that could be avoided using simpler systems such as NMA as a testing ground. We clearly find that even without an actual backbone or side chains the amide unit is experiencing a kind of hydrophobic collapse when exposed to water. This leads to disruption of the long-range ordered HB network between NMA molecules observed in bulk NMA[67] and to clustering of both NMA and water molecules. The resulting spectral dynamics reflecting the HB dynamics, at least in the NMA phase, are "frozen" as compared to the dynamics in the bulk. This suggests that the hydrophobic collapse is an intrinsic property of the amino acid backbone units, which may of course be enhanced by hydrophobic side chains or suppressed by hydrophilic ones.

■ ASSOCIATED CONTENT

Supporting Information

The Supporting Information is available free of charge on the ACS Publications website at DOI: 10.1021/acs.jpca.8b00276.

All possible types of hydrogen bonding between NMA and water and their bundling to the groups; 2D IR spectra of experimental NMA-d_1/D_2O and theoretical NMA−water mixture for both coupled and uncoupled cases; CLS analysis of 2D spectra of the bleaching part (PDF)

■ AUTHOR INFORMATION

Corresponding Author

*E-mail: m.s.pchenitchnikov@rug.nl.

ORCID

Evgeniia Salamatova: 0000-0002-9804-0347
Robbert Bloem: 0000-0001-5854-6733
Thomas L. C. Jansen: 0000-0001-6066-6080
Maxim S. Pshenichnikov: 0000-0002-5446-4287

Present Address

§R.B.: Advanced Research Center for Nanolithography, Science Park 110, 1098 XG Amsterdam, The Netherlands.

Author Contributions

The manuscript was written through contributions of all authors. All authors have given approval to the final version of the manuscript.

Funding

The work in Groningen was supported by the Dieptestrategie Programme of the Zernike Institute for Advanced Materials (University of Groningen, The Netherlands). S.W. kindly acknowledges the John van Geuns Foundation for financial support.

Notes

The authors declare no competing financial interest.

■ ACKNOWLEDGMENTS

We thank Michiel Hilbers for technical support.

■ ABBREVIATIONS

NMA, *N*-Methylacetamide; HB, hydrogen bond; 2D IR, two-dimensional infrared; FTIR, Fourier transform infrared; fwhm, full width at half-maximum; CLS, center line slope; JARDF, joint angular−radial distribution function; RCF, rotational correlation function; RDF, radial distribution function

■ REFERENCES

(1) Hamm, P.; Zanni, M. T. *Concepts and Methods of 2D Infrared Spectroscopy*; Cambridge University Press: Cambridge, U.K., 2011.
(2) Cho, M. *Two-Dimensional Optical Spectroscopy*; CRC Press: Boca Raton, FL, 2009.

DOI: 10.1021/acs.jpca.8b00276
J. Phys. Chem. A 2018, 122, 2468−2478

(3) Cho, M. Coherent Two-Dimensional Optical Spectroscopy. *Chem. Rev.* **2008**, *108*, 1331−1418.
(4) Baiz, C. R.; Reppert, M.; Tokmakoff, A. Introduction to Protein 2D IR Spectroscopy. In *Ultrafast Infrared Vibrational Spectroscopy*; Fayer, M. D., Ed.; Taylor & Francis: New York, 2013; pp 361−404.
(5) Jansen, T. L. C.; Knoester, J. Two-Dimensional Infrared Population Transfer Spectroscopy for Enhancing Structural Markers of Proteins. *Biophys. J.* **2008**, *94*, 1818−1825.
(6) Demirdöven, N.; Khalil, M.; Golonzka, O.; Tokmakoff, A. Correlation Effects in the Two-Dimensional Vibrational Spectroscopy of Coupled Vibrations. *J. Phys. Chem. A* **2001**, *105*, 8025−8030.
(7) Krimm, S.; Bandekar, J. Vibrational Spectroscopy and Conformation of Peptides, Polypeptides, and Proteins. *Adv. Protein Chem.* **1986**, *38*, 181−364.
(8) Hamm, P.; Woutersen, S. Coupling of the Amide I Modes of the Glycine Dipeptide. *Bull. Chem. Soc. Jpn.* **2002**, *75*, 985−988.
(9) Torii, H.; Tasumi, M. Modeling the Amide I Bands of Small Peptides. *J. Chem. Phys.* **1992**, *96*, 3379−3386.
(10) Lessing, J.; Roy, S.; Reppert, M.; Baer, M.; Marx, D.; Jansen, T. L. C.; Knoester, J.; Tokmakoff, A. Identifying Residual Structure in Intrinsically Disordered Systems: A 2D IR Spectroscopic Study of the GVGXPGVG Peptide. *J. Am. Chem. Soc.* **2012**, *134*, 5032−5035.
(11) Smith, A. W.; Lessing, J.; Ganim, Z.; Peng, C. S.; Tokmakoff, A.; Roy, S.; Jansen, T. L. C.; Knoester, J. Melting of β-Hairpin Peptide Using Isotope-Edited 2D IR Spectroscopy and Simulations. *J. Phys. Chem. B* **2010**, *114*, 10913−10924.
(12) Chung, H. S.; Khalil, M.; Smith, A. W.; Ganim, Z.; Tokmakoff, A. Conformational Changes during the Nanosecond-to-Millisecond Unfolding of Ubiquitin. *Proc. Natl. Acad. Sci. U. S. A.* **2005**, *102*, 612−617.
(13) Anfinsen, C. B. Principles That Govern the Folding of Protein Chains. *Science* **1973**, *181*, 223−230.
(14) Selkoe, D. J. Cell Biology of Protein Misfolding: The Examples of Alzheimer's and Parkinson's Diseases. *Nat. Cell Biol.* **2004**, *6*, 1054−1061.
(15) Jaikaran, E. T. A. S.; Clark, A. Islet Amyloid and Type 2 Diabetes: From Molecular Misfolding to Islet Pathophysiology. *Biochim. Biophys. Acta, Mol. Basis Dis.* **2001**, *1537*, 179−203.
(16) Kim, P. S.; Baldwin, R. L. Specific Intermediates in the Folding Reactions of Small Proteins and the Mechanism of Protein Folding. *Annu. Rev. Biochem.* **1982**, *51*, 459−489.
(17) Roder, H.; Elöve, G. A.; Englander, S. W. Structural Characterization of Folding Intermediates in Cytochrome *c* by H-Exchange Labelling and Proton NMR. *Nature* **1988**, *335*, 700−704.
(18) Tirado-Rives, J.; Jorgensen, W. L. Molecular Dynamics Simulations of the Unfolding of an a-Helical Analogue of Ribonuclease A S-Peptide in Water. *Biochemistry* **1991**, *30*, 3864−3871.
(19) Baiz, C. R.; Lin, Y. S.; Peng, C. S.; Beauchamp, K. A.; Voelz, V. A.; Pande, V. S.; Tokmakoff, A. A Molecular Interpretation of 2D IR Protein Folding Experiments with Markov State Models. *Biophys. J.* **2014**, *106*, 1359−1370.
(20) Bycroft, M.; Matouschek, A.; Kellis, J. T., Jr; Serrano, L.; Fersht, A. R. Detection and Characterization of a Folding Intermediate in Barnase by NMR. *Nature* **1990**, *346*, 488−490.
(21) Yang, W. Y.; Pitera, J. W.; Swope, W. C.; Gruebele, M. Heterogeneous Folding of the Trpzip Hairpin: Full Atom Simulation and Experiment. *J. Mol. Biol.* **2004**, *336*, 241−251.
(22) Zhuang, W.; Cui, R. Z.; Silva, D. A.; Huang, X. Simulating the T-Jump-Triggered Unfolding Dynamics of trpzip2 Peptide and Its Time-Resolved IR and Two-Dimensional IR Signals Using the Markov State Model Approach. *J. Phys. Chem. B* **2011**, *115*, 5415−5424.
(23) Hauser, K.; Krejtschi, C.; Huang, R.; Wu, L.; Keiderling, T. A. Site-Specific Relaxation Kinetics of a Tryptophan Zipper Hairpin Peptide Using Temperature-Jump IR Spectroscopy and Isotopic Labeling. *J. Am. Chem. Soc.* **2008**, *130*, 2984−2992.
(24) Balbach, J. Compaction during Protein Folding Studied by Real-Time NMR Diffusion Experiments. *J. Am. Chem. Soc.* **2000**, *122*, 5887−5888.
(25) Muñoz, V.; Thompson, P. A.; Hofrichter, J.; Eaton, W. A. Folding Dynamics and Mechanism of Beta-Hairpin Formation. *Nature* **1997**, *390*, 196−199.
(26) Segel, D. J.; Bachmann, A.; Hofrichter, J.; Hodgson, K. O.; Doniach, S.; Kiefhaber, T. Characterization of Transient Intermediates in Lysozyme Folding with Time-Resolved Small-Angle X-Ray Scattering. *J. Mol. Biol.* **1999**, *288*, 489−499.
(27) Agashe, V. R.; Shastry, M. C. R.; Udgaonkar, J. B. Initial Hydrophobic Collapse in the Folding of Barstar. *Nature* **1995**, *377*, 754−757.
(28) Kühn, T.; Schwalbe, H. Monitoring the Kinetics of Ion-Dependent Protein Folding by Time-Resolved NMR Spectroscopy at Atomic Resolution. *J. Am. Chem. Soc.* **2000**, *122*, 6169−6174.
(29) Ianoul, A.; Mikhonin, A.; Lednev, I. K.; Asher, S. A. UV Resonance Raman Study of the Spatial Dependence of α-Helix Unfolding. *J. Phys. Chem. A* **2002**, *106*, 3621−3624.
(30) Bredenbeck, J.; Helbing, J.; Sieg, A.; Schrader, T.; Zinth, W.; Renner, C.; Behrendt, R.; Moroder, L.; Wachtveitl, J.; Hamm, P. Picosecond Conformational Transition and Equilibration of a Cyclic Peptide. *Proc. Natl. Acad. Sci. U. S. A.* **2003**, *100*, 6452−6457.
(31) Kubelka, J.; Hofrichter, J.; Eaton, W. A. The Protein Folding "Speed Limit.". *Curr. Opin. Struct. Biol.* **2004**, *14*, 76−88.
(32) Yang, W. Y.; Gruebele, M. Detection-Dependent Kinetics as a Probe of Folding Landscape Microstructure. *J. Am. Chem. Soc.* **2004**, *126*, 7758−7759.
(33) Finke, J. M.; Jennings, P. A.; Lee, J. C.; Onuchic, J. N.; Winkler, J. R. Equilibrium Unfolding of the Poly(glutamic acid)20 Helix. *Biopolymers* **2007**, *86*, 193−211.
(34) Wei, G.; Mousseau, N.; Derreumaux, P. Complex Folding Pathways in a Simple β-Hairpin. *Proteins: Struct., Funct., Genet.* **2004**, *56*, 464−474.
(35) Wang, L.; Skinner, J. L. Thermally Induced Protein Unfolding Probed by Isotope-Edited IR Spectroscopy. *J. Phys. Chem. B* **2012**, *116*, 9627−9634.
(36) Meuzelaar, H.; Marino, K. A.; Huerta-Viga, A.; Panman, M. R.; Smeenk, L. E. J.; Kettelarij, A. J.; Van Maarseveen, J. H.; Timmerman, P.; Bolhuis, P. G.; Woutersen, S. Folding Dynamics of the Trp-Cage Miniprotein: Evidence for a Native-like Intermediate from Combined Time-Resolved Vibrational Spectroscopy and Molecular Dynamics Simulations. *J. Phys. Chem. B* **2013**, *117*, 11490−11501.
(37) Beauchamp, K. A.; McGibbon, R.; Lin, Y.-S.; Pande, V. S. Simple Few-State Models Reveal Hidden Complexity in Protein Folding. *Proc. Natl. Acad. Sci. U. S. A.* **2012**, *109*, 17807−17813.
(38) Hartl, F. U. Molecular Chaperones in Cellular Protein Folding. *Nature* **1996**, *381*, 571−580.
(39) Dobson, C. M. Protein Folding and Misfolding. *Nature* **2003**, *426*, 884−890.
(40) Meuzelaar, H.; Tros, M.; Huerta-Viga, A.; Van Dijk, C. N.; Vreede, J.; Woutersen, S. Solvent-Exposed Salt Bridges Influence the Kinetics of α-Helix Folding and Unfolding. *J. Phys. Chem. Lett.* **2014**, *5*, 900−904.
(41) Robson, B.; Pain, R. H. Analysis of the Code Relating Sequence to Conformation in Proteins: Possible Implications for the Mechanism of Formation of Helical Regions. *J. Mol. Biol.* **1971**, *58*, 237−257.
(42) Woutersen, S.; Pfister, R.; Hamm, P.; Mu, Y.; Kosov, D. S.; Stock, G. Peptide Conformational Heterogeneity Revealed from Nonlinear Vibrational Spectroscopy and Molecular-Dynamics Simulations. *J. Chem. Phys.* **2002**, *117*, 6833−6840.
(43) Zanni, M. T.; Asplund, M. C.; Hochstrasser, R. M. Two-Dimensional Heterodyned and Stimulated Infrared Photon Echoes of N-Methylacetamide-D. *J. Chem. Phys.* **2001**, *114*, 4579−4590.
(44) Hamm, P.; Lim, M.; Hochstrasser, R. M. Structure of the Amide I Band of Peptides Measured by Femtosecond Nonlinear-Infrared Spectroscopy. *J. Phys. Chem. B* **1998**, *102*, 6123−6138.
(45) Woutersen, S.; Mu, Y.; Stock, G.; Hamm, P. Hydrogen-Bond Lifetime Measured by Time-Resolved 2D-IR Spectroscopy: N-Methylacetamide in Methanol. *Chem. Phys.* **2001**, *266*, 137−147.
(46) Noda, I.; Liu, Y.; Ozaki, Y. Two-Dimensional Correlation Spectroscopy Study of Temperature-Dependent Spectral Variations of

DOI: 10.1021/acs.jpca.8b00276
J. Phys. Chem. A 2018, 122, 2468−2478

N-Methylacetamide in the Pure Liquid State. 2. Two-Dimensional Infrared Analysis. *J. Phys. Chem.* **1996**, *100*, 8674−8680.
(47) Kwac, K.; Cho, M. Molecular Dynamics Simulation Study of N-Methylacetamide in Water. II. Two-Dimensional Infrared Pump-Probe Spectra. *J. Chem. Phys.* **2003**, *119*, 2256−2263.
(48) DeCamp, M. F.; DeFlores, L.; McCracken, J. M.; Tokmakoff, A.; Kwac, K.; Cho, M. Amide I Vibrational Dynamics of N-Methylacetamide in Polar Solvents: The Role of Electrostatic Interactions. *J. Phys. Chem. B* **2005**, *109*, 11016−11026.
(49) Jansen, T. L. C.; Knoester, J. Nonadiabatic Effects in the Two-Dimensional Infrared Spectra of Peptides: Application to Alanine Dipeptide. *J. Phys. Chem. B* **2006**, *110*, 22910−22916.
(50) Arunan, E.; Desiraju, G. R.; Klein, R. A.; Sadlej, J.; Scheiner, S.; Alkorta, I.; Clary, D. C.; Crabtree, R. H.; Dannenberg, J. J.; Hobza, P.; et al. Definition of the Hydrogen Bond. *Pure Appl. Chem.* **2011**, *83*, 1637−1641.
(51) Chen, X. G.; Schweitzer-Stenner, R.; Krimm, S.; Mirkin, N. G.; Asher, S. A. N-Methylacetamide and Its Hydrogen-Bonded Water Molecules Are Vibrationally Coupled. *J. Am. Chem. Soc.* **1994**, *116*, 11141−11142.
(52) DeFlores, L. P.; Ganim, Z.; Ackley, S. F.; Chung, H. S.; Tokmakoff, A. The Anharmonic Vibrational Potential and Relaxation Pathways of the Amide I and II Modes of N-Methylacetamide. *J. Phys. Chem. B* **2006**, *110*, 18973−18980.
(53) Jansen, T. L. C.; Knoester, J. A Transferable Electrostatic Map for Solvation Effects on Amide I Vibrations and Its Application to Linear and Two-Dimensional Spectroscopy. *J. Chem. Phys.* **2006**, *124*, 044502.
(54) Jansen, T. L. C. Linear Absorption and Two-Dimensional Infrared Spectra of N-Methylacetamide in Chloroform Revisited: Polarizability and Multipole Effect. *J. Phys. Chem. B* **2014**, *118*, 8162−8169.
(55) Jansen, T. L. C.; Dijkstra, A. G.; Watson, T. M.; Hirst, J. D.; Knoester, J. Modeling the Amide I Bands of Small Peptides. *J. Chem. Phys.* **2006**, *125*, 044312.
(56) Bandekar, J. Amide Modes and Protein Conformation. *Biochim. Biophys. Acta, Protein Struct. Mol. Enzymol.* **1992**, *1120*, 123−143.
(57) Schmidt, J. R.; Corcelli, S. A.; Skinner, J. L. Ultrafast Vibrational Spectroscopy of Water and Aqueous N-Methylacetamide: Comparison of Different Electronic Structure/molecular Dynamics Approaches. *J. Chem. Phys.* **2004**, *121*, 8887−8896.
(58) Roseman, M. A. Hydrophobicity of the Peptide C═O···H-N Hydrogen-Bonded Group. *J. Mol. Biol.* **1988**, *201*, 621−623.
(59) Fujisaki, H.; Yagi, K.; Straub, J. E.; Stock, G. Quantum and Classical Vibrational Relaxation Dynamics of N-Methylacetamide on Ab Initio Potential Energy Surfaces. *Int. J. Quantum Chem.* **2009**, *109*, 2047−2057.
(60) Kwac, K.; Cho, M. Molecular Dynamics Simulation Study of N-Methylacetamide in Water. I. Amide I Mode Frequency Fluctuation. *J. Chem. Phys.* **2003**, *119*, 2247−2255.
(61) Fujisaki, H.; Yagi, K.; Hirao, K.; Straub, J. E. Quantum Dynamics of a Peptide-like Molecule Studied by Vibrational Configuration Interaction Method. *Chem. Phys. Lett.* **2007**, *443*, 6−11.
(62) Bastida, A.; Soler, M. A.; Zúñiga, J.; Requena, A.; Kalstein, A.; Fernández-Alberti, S. Hybrid Quantum/Classical Simulations of the Vibrational Relaxation of the Amide I Mode of N-Methylacetamide in D_2O Solution. *J. Phys. Chem. B* **2012**, *116*, 2969−2980.
(63) Farag, M. H.; Bastida, A.; Ruiz-López, M. F.; Monard, G.; Ingrosso, F. Vibrational Energy Relaxation of the Amide I Mode of N-Methylacetamide in D_2O Studied through Born-Oppenheimer Molecular Dynamics. *J. Phys. Chem. B* **2014**, *118*, 6186−6197.
(64) Bloem, R.; Dijkstra, A. G.; Jansen, T. L. C.; Knoester, J. Simulation of Vibrational Energy Transfer in Two-Dimensional Infrared Spectroscopy of Amide I and Amide II Mode in Solution. *J. Chem. Phys.* **2008**, *129*, 055101.
(65) Dijkstra, A. G.; Jansen, T. L. C.; Bloem, R.; Knoester, J. Simulation of Vibrational Energy Transfer in Two-Dimensional Infrared Spectroscopy of Amide I and Amide II Mode in Solution. *J. Chem. Phys.* **2007**, *127*, 194505.
(66) Turton, D. A.; Wynne, K. Structural Relaxation in the Hydrogen-Bonding Liquids N-Methylacetamide and Water Studied by Optical Kerr Effect Spectroscopy. *J. Chem. Phys.* **2008**, *128*, 154516.
(67) Cunha, A. V.; Salamatova, E.; Bloem, R.; Roeters, S. J.; Woutersen, S.; Pshenichnikov, M. S.; Jansen, T. L. C. Interplay between Hydrogen Bonding and Vibrational Coupling in Liquid N-Methylacetamide. *J. Phys. Chem. Lett.* **2017**, *8*, 2438−2444.
(68) Chuntonov, L.; Kumar, R.; Kuroda, D. G. Non-Linear Infrared Spectroscopy of the Water Bending Mode: Direct Experimental Evidence of Hydration Shell Reorganization? *Phys. Chem. Chem. Phys.* **2014**, *16*, 13172−13181.
(69) Chang, R. *Chemistry*; McGraw-Hill Companies: New York, 2009.
(70) Helbing, J.; Hamm, P. Compact Implementation of Fourier Transform Two-Dimensional IR Spectroscopy without Phase Ambiguity. *J. Opt. Soc. Am. B* **2011**, *28*, 171−178.
(71) Bloem, R.; Garrett-Roe, S.; Strzalka, H.; Hamm, P.; Donaldson, P. Enhancing Signal Detection and Completely Eliminating Scattering Using Quasi-Phase-Cycling in 2D IR Experiments. *Opt. Express* **2010**, *18*, 27067−27078.
(72) Backus, E. H. G.; Garrett-Roe, S.; Hamm, P. Phasing Problem of Heterodyne-Detected Two-Dimensional Infrared Spectroscopy. *Opt. Lett.* **2008**, *33*, 2665−2667.
(73) Van Der Spoel, D.; Lindahl, E.; Hess, B.; Groenhof, G.; Mark, A. E.; Berendsen, H. J. C. GROMACS: Fast, Flexible, and Free. *J. Comput. Chem.* **2005**, *26*, 1701−1718.
(74) Jorgensen, W. L.; Maxwell, D. S.; Tirado-Rives, J. Development and Testing of the OLPS All-Atom Force Field on Conformational Energetics and Properties of Organic Liquids. *J. Am. Chem. Soc.* **1996**, *118*, 11225−11236.
(75) Berendsen, H. J. C.; Grigera, J. R.; Straatsma, T. P. The Missing Term in Effective Pair Potentials. *J. Phys. Chem.* **1987**, *91*, 6269−6271.
(76) Swope, W. C.; Andersen, H. C.; Berens, P. H.; Wilson, K. R. A Computer Simulation Method for the Calculation of Equilibrium Constants for the Formation of Physical Clusters of Molecules: Application to Small Water Clusters. *J. Chem. Phys.* **1982**, *76*, 637−649.
(77) Tobias, D. J.; Brooks, C. L., III; Fleischman, S. H. Conformational Flexibility in Free Energy Simulations. *Chem. Phys. Lett.* **1989**, *156*, 256−260.
(78) Caleman, C.; Van Maaren, P. J.; Hong, M.; Hub, J. S.; Costa, L. T.; Van Der Spoel, D. Force Field Benchmark of Organic Liquids: Density, Enthalpy of Vaporization, Heat Capacities, Surface Tension, Isothermal Compressibility, Volumetric Expansion Coefficient, and Dielectric Constant. *J. Chem. Theory Comput.* **2012**, *8*, 61−74.
(79) Hess, B.; Bekker, H.; Berendsen, H. J. C.; Fraaije, J. G. E. M. LINCS: A Linear Constraint Solver for Molecular Simulations. *J. Comput. Chem.* **1997**, *18*, 1463−1472.
(80) Liang, C.; Jansen, T. L. C. An Efficient N^3-Scaling Propagation Scheme for Simulating Two-Dimensional Infrared and Visible Spectra. *J. Chem. Theory Comput.* **2012**, *8*, 1706−1713.
(81) Cunha, A. V.; Bondarenko, A. S.; Jansen, T. L. C. Assessing Spectral Simulation Protocols for the Amide I Band of Proteins. *J. Chem. Theory Comput.* **2016**, *12*, 3982−3992.
(82) Kumar, R.; Schmidt, J. R.; Skinner, J. L. Hydrogen Bonding Definitions and Dynamics in Liquid Water. *J. Chem. Phys.* **2007**, *126*, 204107.
(83) Luzar, A.; Chandler, D. Hydrogen-Bond Kinetics in Liquid Water. *Nature* **1996**, *379*, 55−57.
(84) Torres, J.; Briggs, J. A. G.; Arkin, I. T. Multiple Site-Specific Infrared Dichroism of CD3-ζ, a Transmembrane Helix Bundle. *J. Mol. Biol.* **2002**, *316*, 365−374.
(85) Woutersen, S.; Mu, Y.; Stock, G.; Hamm, P. Subpicosecond Conformational Dynamics of Small Peptides Probed by Two-Dimensional Vibrational Spectroscopy. *Proc. Natl. Acad. Sci. U. S. A.* **2001**, *98*, 11254−11258.
(86) Pshenichnikov, M. S.; Yeremenko, S.; Wiersma, D. A. IR Photon-Echo Spectroscopy of Water: The Thermalization Effects. *Springer Ser. Chem. Phys.* **2005**, *79*, 404−406.

DOI: 10.1021/acs.jpca.8b00276
J. Phys. Chem. A 2018, 122, 2468−2478

(87) Cringus, D.; Bakulin, A.; Lindner, J.; Vöhringer, P.; Pshenichnikov, M. S.; Wiersma, D. A. Ultrafast Energy Transfer in Water - AOT Reverse Micelles. *J. Phys. Chem. B* **2007**, *111*, 14193−14207.
(88) Kwak, K.; Park, S.; Finkelstein, I. J.; Fayer, M. D. Frequency-Frequency Correlation Functions and Apodization in Two-Dimensional Infrared Vibrational Echo Spectroscopy: A New Approach. *J. Chem. Phys.* **2007**, *127*, 124503.
(89) Kwak, K.; Rosenfeld, D. E.; Fayer, M. D. Taking Apart the Two-Dimensional Infrared Vibrational Echo Spectra: More Information and Elimination of Distortions. *J. Chem. Phys.* **2008**, *128*, 204505.
(90) Woys, A. M.; Almeida, A. M.; Wang, L.; Chiu, C. C.; McGovern, M.; De Pablo, J. J.; Skinner, J. L.; Gellman, S. H.; Zanni, M. T. Parallel β-Sheet Vibrational Couplings Revealed by 2D IR Spectroscopy of an Isotopically Labeled Macrocycle: Quantitative Benchmark for the Interpretation of Amyloid and Protein Infrared Spectra. *J. Am. Chem. Soc.* **2012**, *134*, 19118−19128.
(91) Bakulin, A. A.; Cringus, D.; Pieniazek, P. A.; Skinner, J. L.; Jansen, T. L. C.; Pshenichnikov, M. S. Dynamics of Water Confined in Reversed Micelles: Multidimensional Vibrational Spectroscopy Study. *J. Phys. Chem. B* **2013**, *117*, 15545−15558.
(92) Bakulin, A. A.; Liang, C.; Jansen, T. L. C.; Wiersma, D. A.; Bakker, H. J.; Pshenichnikov, M. S. Hydrophobic Solvation: A 2D IR Spectroscopic Inquest. *Acc. Chem. Res.* **2009**, *42*, 1229−1238.
(93) Jansen, T. L. C.; Auer, B. M.; Yang, M.; Skinner, J. L. Two-Dimensional Infrared Spectroscopy and Ultrafast Anisotropy Decay of Water. *J. Chem. Phys.* **2010**, *132*, 224503.
(94) Groot, C. C. M.; Meister, K.; DeVries, A. L.; Bakker, H. J. Dynamics of the Hydration Water of Antifreeze Glycoproteins. *J. Phys. Chem. Lett.* **2016**, *7*, 4836−4840.
(95) Fogarty, A. C.; Laage, D. Water Dynamics in Protein Hydration Shells: The Molecular Origins of the Dynamical Perturbation. *J. Phys. Chem. B* **2014**, *118*, 7715−7729.
(96) Daley, K. R.; Kubarych, K. J. An "iceberg" Coating Preserves Bulk Hydration Dynamics in Aqueous PEG Solutions. *J. Phys. Chem. B* **2017**, *121*, 10574−10582.
(97) Yang, J.; Wang, Y.; Wang, L.; Zhong, D. Mapping Hydration Dynamics around a β-Barrel Protein. *J. Am. Chem. Soc.* **2017**, *139*, 4399−4408.
(98) Tros, M.; Zheng, L.; Hunger, J.; Bonn, M.; Bonn, D.; Smits, G. J.; Woutersen, S. Picosecond Orientational Dynamics of Water in Living Cells. *Nat. Commun.* **2017**, *8*, 904.
(99) Thouless, D. J. Electrons in Disordered Systems and the Theory of Localization. *Phys. Rep.* **1974**, *13*, 93−142.
(100) Wynne, K. The Mayonnaise Effect. *J. Phys. Chem. Lett.* **2017**, *8*, 6189−6192.

DOI: 10.1021/acs.jpca.8b00276
J. Phys. Chem. A 2018, 122, 2468−2478